Metabolic potential of uncultured bacteria and archaea associated with petroleum seepage in deep-sea sediments

Xiyang Dong [1,*], Chris Greening [2], Jayne E. Rattray [1], Anirban Chakraborty [1], Maria Chuvochina [2], Daisuke Mayumi [1,3], Jan Dolfing [4], Carmen Li [1], James M. Brooks [5], Bernie B. Bernard [5], Ryan A. Groves[1], Ian A. Lewis [1], Casey R.J. Hubert [1,*]

[1] Department of Biological Sciences, University of Calgary, Calgary, T2N 1N4, Canada

[2] School of Biological Sciences, Monash University, Clayton, VIC 3800, Australia

[3] Institute for Geo-Resources and Environment, Geological Survey of Japan, National Institute of Advanced Industrial Science and Technology (AIST), 1-1-1 Higashi, Tsukuba, 305-8567, Japan

[4] School of Engineering, Newcastle University, Newcastle upon Tyne, NE1 7RU, United Kingdom

[5] TDI Brooks International, College Station, Texas, TX 77845, USA

* Corresponding authors. E-mail: xiyang.dong@ucalgary.ca (X. Dong), chubert@ucalgary.ca (C. R.J. Hubert).

The authors declare no conflict of interest.

Abstract

The lack of microbial genomes and isolates from the deep seabed means that very little is known about the ecology of this vast habitat. Here, we investigated energy and carbon acquisition strategies of microbial communities from three deep seabed petroleum seeps (3 km water depth) in the Eastern Gulf of Mexico. Shotgun metagenomic analysis revealed that each sediment harbored diverse communities of chemoheterotrophs and chemolithotrophs. We recovered 82 metagenome-assembled genomes affiliated with 21 different archaeal and bacterial phyla. Multiple genomes encoded enzymes for anaerobic oxidation of aliphatic and aromatic compounds, including those of candidate phyla Aerophobetes, Aminicenantes, TA06 and Bathyarchaeota. Microbial interactions are predicted to be driven by acetate and molecular hydrogen. These findings are supported by sediment geochemistry, metabolomics, and thermodynamic modelling. Overall, we infer that deep-sea sediments experiencing thermogenic hydrocarbon inputs harbor phylogenetically and functionally diverse communities potentially sustained through anaerobic hydrocarbon, acetate and hydrogen metabolism.

Deep-sea sediments, generally understood to be those occurring in water depths greater than ~500 meters, represent one of the largest habitats on Earth. In recent years, culture-independent 16S rRNA gene surveys and metagenomic studies have revealed these sediments host a vast abundance and diversity of bacteria and archaea [1-8]. Cell numbers decrease with sediment depth and age, from between 10^6 and 10^{10} cm^{-3} in the upper cm at the sediment-water interface to below 10^4 cm^{-3} several kilometers below the ocean floor [9, 10]. However, due to a lack of cultured representatives and genomes recovered from deep-sea sediments, it remains largely unresolved how microorganisms survive and function in these nutrient-limited ecosystems. Energy and carbon sources are essential requirements that allow the buried microorganisms to persist. With sunlight not reaching the deep seabed, photosynthetic processes do not directly support these communities [11]. It has therefore been proposed that deep sea benthic and subseafloor microbes are primarily sustained by complex detrital organic matter, including carbohydrates, proteinaceous compounds, and humic substances, derived from the overlying water column *via* sedimentation [11-13].

Another important potential carbon and energy sources in deep-sea sediments are petroleum geofluids that migrate from subsurface reservoirs up to the seafloor [14]. Petroleum compounds include smaller gaseous molecules, such as methane, propane, and butane, and larger aliphatic and aromatic liquids. Numerous studies have investigated the role of methane oxidation in seabed sediments, which is mediated by anaerobic methanotrophic archaea (ANME), generally in syntrophy with bacteria respiring sulfate or other electron acceptors [4, 6, 8, 15, 16]. In contrast, little is known about the degradation of larger alkanes or aromatic compounds by deep seabed microorganisms. Vigneron et al. [2] performed a comparative gene-centric study of hydrocarbon and methane seeps in the Gulf of Mexico, and suggested that microorganisms in deep cold seeps

(water depth ~1 km) can potentially utilize a range of non-methane hydrocarbons. However, due to the absence of metagenome binning in that study, relevant metabolic functions were not assigned to specific pathways or taxa.

In addition to organic carbon compounds, microbial life in deep-sea sediments is also supported by inorganic electron donors. Some microorganisms have been isolated from deep sediments that are able to sustain themselves by oxidizing elemental sulfur, hydrogen sulfide, carbon monoxide, ammonia, and molecular hydrogen (H_2) [6, 8, 11]. Of these, H_2 is a particularly important energy source given its production in large quantities by biological and geochemical processes. H_2 can be generated as a metabolic byproduct of fermentation, together with volatile fatty acids such as acetate, during organic matter degradation [9, 17]. H_2 can also be produced abiotically via serpentinization, radiolysis of water, or thermal alteration of sedimentary organic matter [18]. For example, the radiolysis of water by naturally occurring radionuclides (*e.g.* ^{40}K and ^{238}U) is estimated to produce 10^{11} mol H_2 per year [8, 19]. Depending on the availability of electron acceptors, H_2 oxidation can be coupled to sulfate, nitrate, metal, and organohalide respiration, as well as acetogenesis and methanogenesis [8, 11].

In this study, we used culture-independent approaches to study the role of microbial communities in the degradation of organic matter, including both detrital biomass and petroleum hydrocarbons. We performed metagenomic, geochemical and metabolomic analyses of deep seabed sediments (water depth ~3 km). Samples were chosen from three sites exhibiting evidence of different levels of migrated thermogenic hydrocarbons. Metagenomes generated from sediment samples of each site were assembled and binned to obtain metagenome-assembled genomes (MAGs) and to reconstruct metabolic pathways for dominant members of the microbial

77 communities. Complementing this genome-resolved metagenomics, a gene-centric analysis was
78 performed by directly examining unassembled metagenomic data. Through the combination of
79 metagenomics with geochemistry and metabolomics, supported by thermodynamic modeling, we
80 provide evidence that (1) deep-sea sediments harbor phylogenetically diverse heterotrophic and
81 lithotrophic microbial communities; (2) some members from the candidate phyla are engaged in
82 degradation of aliphatic and aromatic compounds; and (3) microbial community members are
83 likely interconnected *via* acetate and hydrogen metabolism.

84 **Results**

85 **Hydrocarbon migration in seabed sediments**

86 This study tested three petroleum-associated near-surface sediments (referred to as Sites E26,
87 E29 and E44; see map in Supplementary Figure 1) sampled from the Eastern Gulf of Mexico [20].
88 Migrated thermogenic hydrocarbon content in the piston cores was analyzed for each of the three
89 sites (Table 1). All three sediments contained high concentrations of aromatic compounds and
90 liquid alkanes; aromatic compounds were most abundant at Site E26, while liquid alkanes were
91 on average 2.5-fold higher concentration at Sites E26 and E29 than Site E44. Alkane gases were
92 only abundant at Site E29 and were almost exclusively methane (CH_4). CH_4 sources can be
93 inferred from stable isotopic compositions of CH_4 and molar ratios of CH_4 to higher
94 hydrocarbons [15]. Ratios of $C_1/(C_2+C_3)$ were greater than 1,000 and $\delta^{13}C$ values of methane were
95 more negative than -60‰, indicating that the CH_4 in these sediments was predominantly
96 biogenic [15, 21]. Similar co-occurrence of biogenic methane and complex hydrocarbons have been
97 reported in a nearby seep in the Mississippi Canyon in the Gulf of Mexico [22]. GC-MS revealed
98 an unresolved complex mixture (UCM) of saturated hydrocarbons in the C_{15+} range in all three

sites. Such UCM signals correspond to degraded petroleum hydrocarbons and may indicate the occurrence of oil biodegradation at these sites [23].

Phylogenetically diverse bacterial and archaeal communities

Illumina NextSeq sequencing of genomic DNA from deep-sea sediment communities produced 85,825,930, 148,908,270, and 138,795,692 quality-filtered reads for Sites E26, E29, and E44, respectively (Supplementary Table 1). The 16S rRNA gene amplicon sequencing results suggest that the sediments harbor diverse bacterial and archaeal communities, with Chao1 richness estimates of 359, 1375 and 360 amplicon sequence variants (ASVs) using bacterial-specific primers, and 195, 180 and 247 ASVs using archaeal-specific primers, for Sites E26, E29 and E44, respectively (Supplementary Table 2 and Supplementary Figure 2). In accordance with amplicon sequencing results, taxonomic profiling of metagenomes using small subunit ribosomal RNA (SSU rRNA) marker genes demonstrated that the most abundant phyla in the metagenomes were, in decreasing order, Chloroflexi (mostly classes *Dehalococcoidia* and *Anaerolineae*), *Candidatus* Atribacteria, Proteobacteria (mostly class *Deltaproteobacteria*), and *Candidatus* Bathyarchaeota (Supplementary Table 3 and Figure 1a). While the three sites share a broadly similar community composition, notable differences were *Ca.* Bathyarchaeota and Proteobacteria being in higher relative abundance at the sites associated with more hydrocarbons (E29 and E26; Table 1), whereas the inverse is true for Actinobacteria, the Patescibacteria group, and *Ca.* Aerophobetes that are all present in higher relative abundance at Site E44 where associated hydrocarbon levels are lower. Additional sampling is required to determine whether these differences are due to the presence of hydrocarbons or other factors.

Assembly and binning for the three metagenomes resulted in a total of 82 MAGs with >50% completeness and <10% contamination based on CheckM analysis [24]. Reconstructed MAGs comprise taxonomically diverse members from a total of six archaeal and 15 bacterial phyla (Figure 2 and Supplementary Table 4). Within the domain Bacteria, members of the phylum Chloroflexi are highly represented in each sample, especially from the classes *Dehalococcoidia* and *Anaerolineae*. Within the domain Archaea, members of phylum Bathyarchaeota were recovered from all three sites. Most other MAGs belong to poorly understood candidate phyla that lack cultured representatives, including Aminicenantes (formerly OP8), Aerophobetes (formerly CD12), Cloacimonas (formerly WWE1), Stahlbacteria (formerly WOR-3), Atribacteria (formerly JS1 and OP9), TA06 (Supplementary Note 1 and Supplementary Table 5), and the Asgard superphylum, including Lokiarchaeota, Thorarchaeota, and Heimdallarchaeota.

In summary, while there are considerable community-level differences between the three sample locations, the recovered MAGs share common taxonomic affiliations at the phylum and class levels. Guided by associated geochemistry from the three sediment cores (Table 1 and Supplementary Note 2), we subsequently analyzed the metabolic potential of these MAGs to understand how bacterial and archaeal community members generate energy and biomass in these natural petroleum-associated deep-sea environments. Hidden Markov models (HMMs) and homology-based models were used to search for the presence of different metabolic genes in both the recovered MAGs and unbinned metagenomes. Where appropriate, findings were further validated through metabolomic analyses, phylogenetic visualization, and analysis of gene context.

Detrital biomass and hydrocarbon degradation

In deep-sea marine sediments, organic carbon is supplied either as detrital matter from the overlying water column or as aliphatic and aromatic petroleum compounds that migrate upwards from underlying petroleum-bearing sediments [11]. With respect to detrital matter, genes involved in carbon acquisition and breakdown were prevalent across both archaeal and bacterial MAGs. These include genes encoding intracellular and extracellular carbohydrate-active enzymes and peptidases, as well as relevant transporters and glycolysis enzymes (Figure 3 and Supplementary Table 6). The ability to break down fatty acids and other organic acids *via* the beta-oxidation pathway was identified in 13 MAGs, including members of Chloroflexi, *Deltaproteobacteria*, Aerophobetes and Lokiarchaeota (Figure 3 and Supplementary Table 6). Metabolomics data supported these genomic predictions and showed a surprising degree of consistency between the geographically distinct sampling sites (Figure 4). Over 50 metabolites from eight pathways were detected in all the samples, including carbohydrate metabolism (*e.g.* glucose), amino acid metabolism (*e.g.* glutamate), and beta oxidation (*e.g.* 10-hydroxydecanoate). Together, the metagenomic and metabolomic data suggest that seabed microorganisms are involved in recycling of residual organic matter, including complex carbohydrates, proteins and lipids.

To identify the potential for microbial degradation of hydrocarbons, we focused on functional marker genes encoding enzymes that initiate anaerobic hydrocarbon biodegradation by activating mechanistically stable C-H bonds [25]. We obtained evidence that two of the four known pathways for oxygen-independent C-H activation [25-28] were present: hydrocarbon addition to fumarate by glycyl-radical enzymes [28] and hydroxylation with water by molybdenum cofactor-containing enzymes [25]. Glycyl-radical enzymes proposed to mediate hydrocarbon addition to fumarate were

found in 13 MAGs (Chloroflexi, Aminicenantes, Aerophobetes, Actinobacteria, Bathyarchaeota, Thorarchaeota and Lokiarchaeota) (Figure 3). The sequences identified are phylogenetically distant from canonical akyl-/arylalkylsuccinate synthases, but form a common clade with the glycyl-radical enzymes proposed to mediate alkane activation in anaerobic alkane degraders *Vallitalea guaymasensis* L81 and *Archaeoglobus fulgidus* VC-16 [29-31] (Supplementary Figure 3). Based on quality-filtered reads, canonical AssA (n-alkane succinate synthase) and BssA (benzyl succinate synthase) enzymes are also encoded at these sites and were most abundant in Site E29 (Supplementary Table 7). In agreement with this, metabolomics analysis detected six succinic acid conjugates involved in hydrocarbon activation, including conjugates of xylene, toluene, cyclohexane, and isopropane (Figure 4). For the hydroxylation pathway, a *Dehalococcoidia* MAG in Site E29 encoded proteins sharing over 40% sequence identities to the catalytic subunits of *p*-cymene dehydrogenase (Cmd) and alkane C_2-methylene hydroxylase (Ahy) (Figure 3 and Supplementary Figure 4) [32]. Genes encoding enzymes catalyzing hydrocarbon carboxylation (*ubiD*-like), reverse methanogenesis (*mcrA*-like), and aerobic hydrocarbon degradation (*e.g. alkB*) were not detected (Supplementary Table 7). The latter result is expected due to the low concentrations of oxygen in the top 20 cm of organic rich seabed sediments [11].

Our results also provide evidence that aromatic compounds can be anaerobically degraded *via* channeling into the central benzoyl-CoA degradation pathway. Through metabolomic analysis, we detected multiple intermediates (Figure 4) involved in both the production and degradation of benzoyl-CoA, a universal intermediate formed during the degradation of aromatic compounds [33]. Various compounds that can be activated to form benzoyl-CoA were detected, including benzoate, benzylsuccinate, 4-hydroxybenzoate, phenylacetate, acetophenone, and phenol. The downstream metabolite glutarate was also highly abundant (Figure 4). Benzoyl-CoA can be

reduced to cyclohex-1,5-diene-1-carboxyl-CoA by either the Class I ATP-dependent benzoyl-CoA reductase pathway (*bcr* genes, *e.g. Thauera aromatica*) or Class II ATP-independent reductase (*bam* genes, *e.g.* sulfate reducers) [34]. We identified *bcr* genes for the Class I pathways in 12 MAGs from both bacteria (*i.e.*, *Dehalococcoidia*, *Anaerolineae*, *Deltaproteobacteria*, Aminicenantes and TA06) and archaea (*i.e.*, *Thermoplasmata* and Bathyarchaeota) (Figure 3 and Supplementary Figure 5). Genes for further transformation of dienoyl-CoA to 3-hydroxypimelyl-CoA were also identified, *i.e.* those encoding 6-oxo-cyclohex-1-ene-carbonyl-CoA hydrolase (*oah*), cyclohex-1,5-diencarbonyl-CoA hydratase (*dch*) and 6-hydroxycyclohex-1-ene-1-carbonyl-CoA dehydrogenases (*had*) [35] (Supplementary Figure 5). In combination, these results strongly suggest that the organisms represented by these MAGs mediate the typical downstream degradation of aromatic compounds through the central benzoyl-CoA Bcr-Dch-Had-Oah pathway. However, sources of benzoate other than via anaerobic degradation of the above compounds, cannot be ruled out based on current data.

Production and consumption of acetate and hydrogen

Analysis of MAGs from these deep-sea hydrocarbon-associated sediments suggests that fermentation, rather than respiration, is the primary mode of organic carbon turnover in these environments. Most recovered MAGs with capacity for heterotrophic carbon degradation lacked respiratory primary dehydrogenases and terminal reductases, with exception of several Proteobacteria and one Chloroflexi (Supplementary Table 6). In contrast, various MAGs contained genes indicating the capability for fermentative production of acetate (69 MAGs), lactate (14 MAGs), and ethanol (6 MAGs) (Figure 3 and Supplementary Table 6). These findings therefore provide genomic evidence supporting other studies emphasizing the importance of

208 fermentation, including acetate production, in deep-sea sediments [12, 36]. Acetate can also be
209 produced by acetogenic CO_2 reduction through the Wood-Ljungdahl pathway using a range of
210 inorganic and organic substrates [15]. Partial or complete sets of genes for the Wood-Ljungdahl
211 pathway were found in 50 MAGs (Figure 3 and Supplementary Figure 6), including those
212 affiliated with phyla previously inferred to mediate acetogenesis in deep-sea sediments through
213 either the tetrahydrofolate-dependent bacterial pathway (*e.g.* Chloroflexi and Aerophobetes) [7, 37]
214 or the tetrahydromethanopterin-dependent archaeal variant (*e.g.* Bathyarchaeota and Asgard
215 group) [38, 39]. In addition, the signature diagnostic gene for the Wood-Ljungdahl pathway (*acsB*;
216 acetyl-CoA synthase) is in high relative abundance in the quality-filtered metagenome reads at
217 all three sites (Supplementary Table 7). The most abundant MAG at each site were all putative
218 acetogenic heterotrophs, *i.e. Dehalococcoidia* E26_bin16, Actinobacteria E44_bin5, and
219 Aminicenantes E29_bin47 for Sites E26, E44 and E29 respectively (~3.3-4.5% relative
220 abundance, Supplementary Table 4). These observations are in agreement with mounting
221 evidence that homoacetogens play a quantitatively important role in organic carbon cycling in
222 the marine deep biosphere [38, 40, 41].

223 The potential for H_2 metabolism was also found in MAGs from all three sites. We screened
224 putative hydrogenase genes from various subgroups in MAGs as well as unbinned metagenomic
225 sequences (Figures 1, 3 and Supplementary Tables 6-7). Surprisingly few H_2 evolving-only
226 hydrogenases were observed, with only five Group A [FeFe]-hydrogenases and five Group 4
227 [NiFe]-hydrogenases detected across the bacterial and archaeal MAGs. Instead, the most
228 abundant hydrogenases within the MAGs and quality-filtered unassembled reads were the Group
229 3b, 3c, and 3d [NiFe]-hydrogenases. Group 3b and 3d hydrogenases are physiologically
230 reversible, but generally support fermentation in anoxic environments by coupling NAD(P)H

231 reoxidation to fermentative H_2 evolution [42-44]. Group 3c hydrogenases mediate a central step in
232 hydrogenotrophic methanogenesis, bifurcating electrons from H_2 to heterodisulfides and
233 ferredoxin [45]; their functional role in bacteria and non-methanogenic archaea remains unresolved
234 [44] yet corresponding genes frequently co-occur with heterodisulfide reductases across multiple
235 archaeal and bacterial MAGs (Figure 3). Various Group 1 [NiFe]-hydrogenases were also
236 detected, which are known to support hydrogenotrophic respiration in conjunction with a wide
237 range of terminal reductases. This is consistent with previous studies in the Gulf of Mexico that
238 experimentally measured the potential for hydrogen oxidation catalyzed by hydrogenase
239 enzymes [46].

240 Given the genomic evidence for hydrogen and acetate production in these sediments, we
241 investigated whether any of the MAGs encoded terminal reductases to respire these compounds.
242 In agreement with porewater sulfate concentrations (16-27 mM; see Supplementary Note 2), the
243 key genes for dissimilatory sulfate reduction (*dsrAB*) were widespread across the metagenome
244 reads, particularly at Site E29 (Supplementary Table 7); however, probably due to
245 incompleteness of genomes or insufficient binning, these genes were identified only in two
246 MAGs affiliated with *Deltaproteobacteria* and *Dehalococcoidia* (Supplementary Table 6). We
247 also identified 31 putative reductive dehalogenase genes (*rdhA*) across 22 MAGs, mainly from
248 Aminicenantes and Bathyarchaeota (Figure 3 and Supplementary Table 6); this suggests that
249 organohalides, which can be produced through abiotic and biotic processes in marine ecosystems
250 [47], may be electron acceptors in these deep-sea sediments. At least two thirds of the MAGs
251 corresponding to putative sulfate reducers and dehalorespirers encoded the capacity to
252 completely oxidize acetate and other organic acids to CO_2 using either the reverse Wood-
253 Ljungdahl pathway or TCA cycle (Figure 3 and Supplementary Table 6). Several of these MAGs

254 also harbored the capacity for hydrogenotrophic dehalorespiration *via* Group 1a and 1b [NiFe]-
255 hydrogenases (Figure 3). In addition to these dominant uptake pathways, one MAG belonging to
256 the epsilonproteobacterial genus *Sulfurovum* (E29_bin29) included genes for the enzymes
257 needed to oxidize either H_2 (group 1b [NiFe]-hydrogenase), elemental sulfur (*soxABXYZ*), and
258 sulfide (*sqr*), using nitrate as an electron acceptor (*napAGH*); this MAG also has a complete set
259 of genes for autotrophic CO_2 fixation *via* the reductive TCA cycle (Figure 3 and Supplementary
260 Table 6).

261 The capacity for methanogenesis appears to be relatively low. The genes for methanogenesis
262 were detected in quality-filtered unassembled reads in all three sediments and were mainly
263 affiliated with acetoclastic methanogens at Site E29, and hydrogenotrophic methanogens at the
264 other two sites (Figure 1d). However, none of the MAGs contained *mcrA* genes. Overall, the
265 collectively weak *mcrA* signal in the metagenomes suggests that the high levels of biogenic
266 methane detected by geochemical analysis (Table 1) is due to methanogenesis in deeper
267 sediment layers. Similar phenomena have been observed in other sites, where *mcrA* genes are in
268 low abundance despite clear geochemical evidence for biogenic methane [48]. Sequencing
269 additional sediment depths at greater resolution would likely result in detection of *mcrA*-related
270 methanogens and ANME lineages.

271 **Thermodynamic modelling**

272 Together, the geochemical, metabolomic, and metagenomic data strongly indicate that anaerobic
273 degradation of aliphatic and aromatic compounds occurs in these deep-sea sediments (Table 1
274 and Figures 3-4). Recreating the environmental conditions for cultivating the organisms
275 represented by the retrieved MAGs is a challenging process, preventing further validation of the

degradation capabilities of these compounds (and other metabolisms) among the majority of the lineages represented by the MAGs retrieved here [41]. Instead, we provide theoretical evidence that anaerobic degradation of aliphatic and aromatic compounds is feasible in this environment by modelling whether these processes are thermodynamically favorable in the conditions typical of deep-sea sediments, namely high pressure and low temperature.

As concluded from the genome analysis and supported by metabolomics (Figures 3-4), it is likely that anaerobic degradation occurs through an incomplete oxidation pathway. However, due to incompleteness of the reconstructed genomes, we cannot exclude the possibility that complete oxidation of aliphatic and aromatic compounds to CO_2 occurs through, for example, coupling with sulfate reduction (Figure 3). Additionally, several recent studies indicate that some aliphatic and aromatic compounds can be incompletely oxidized to acetate *via* the Wood-Ljungdahl pathway [37, 40, 49]. Therefore, we compared the thermodynamic constraints on anaerobic biodegradation for three plausible scenarios (Table 2): (i) incomplete oxidation with production of hydrogen and acetate, (ii) acetogenic oxidation with production of acetate alone, and (iii) complete oxidation coupled with sulfate reduction. Hexadecane and benzoate are used as representative aliphatic and aromatic compounds, respectively, based on the results of geochemistry and metabolomics results (*e.g.* C_{2+} alkane and benzoate detection) and genomic analysis (*e.g.* genes encoding for glycyl-radical enzymes and *bcr* genes). Under deep-sea conditions, without taking the *in situ* concentrations of hydrogen and acetate into consideration, the calculations show that sulfate-dependent complete oxidation of hexadecane and benzoate, as well as acetogenic oxidation of benzoate, would be energetically favorable. The three other reactions would be endergonic under most conditions, but based on the measured concentrations for both acetate and H_2 in these sediments being low (Supplementary Note 2) these reactions

could also take place in theory (Table 2 and Figure 5). This suggests that acetate- and H_2-scavengers, by making acetogenic and hydrogenogenic degradation more thermodynamically favorable, may support activity of anaerobic degraders in the community.

Discussion

In this study, metagenomics revealed that most of the bacteria and archaea in the deep-sea sediment microbial communities sampled belong to candidate phyla that lack cultured representatives and sequenced genomes (Figures 1 and 2). As a consequence, it is challenging to link phylogenetic patterns with the microbial functional traits underpinning the biogeochemistry of deep seabed habitats. Here, we were able to address this by combining *de novo* assembly and binning of metagenomic data with petroleum geochemistry, metabolite identification, and thermodynamic modeling. Pathway reconstruction from 82 MAGs recovered from the three deep-sea near surface sediments revealed that many community members were capable of acquiring and hydrolyzing residual organic matter (Figure 3), whether supplied as detritus from the overlying water column or as autochthonously produced necromass. Heterotrophic fermenters and acetogens were in considerably higher relative abundance than heterotrophic respirers, despite the abundance of sulfate in the sediments (Supplementary Note 2). For example, while genomic coverage of putative sulfate reducers is relatively low (< 1% of the communities), putative acetogenic heterotrophs were the most abundant community members at each site. Therefore, microbial communities in the deep seabed are likely shaped more by the capacity to utilize available electron donors than by the availability of oxidants. In line with the different geochemical profiles at the three sites (Table 1), some differences in the composition of microbial communities and the abundance of key metabolic genes were observed (Figure 1 and

Supplementary Table 7). However, metabolic capabilities such as fermentation, acetogenesis, and hydrogen metabolism were conserved across diverse phyla in each site (Figure 3). This suggests some functional redundancy in these microbial communities, similar to that recently inferred in a study of Guaymas Basin hydrothermal sediments [50].

In this context, multiple lines of evidence indicate aliphatic or aromatic compounds serve as carbon and energy sources for anaerobic populations in these deep-sea hydrocarbon seep environments (Tables 1 - 2; Figures 3 - 5). Whereas capacity for detrital organic matter degradation is a common feature in the genomes retrieved in this study, and from many other environments in general [51], anaerobic degradation of aliphatic or aromatic compounds is a more exclusive feature that was detected in 19 out of 82 MAGs. In all three sediments, there was metagenomic and metabolomic evidence for anaerobic hydrocarbon oxidation *via* hydrocarbon addition to fumarate and hydroxylation pathways, as well as anaerobic aromatic compound degradation by the Class I benzoyl-CoA reductase pathway. The ability to utilize aliphatic or aromatic compounds may explain the ecological dominance (high relative abundance) of certain lineages of bacteria and archaea in these microbial communities (Figure 1a). Many of the detected phyla have previously been found to be associated with hydrocarbons in various settings. For example, Aerophobetes have been detected in other cold seep environments [7], Aminicenantes are often found associated with fossil fuels [52], and Chloroflexi harboring genes for anaerobic hydrocarbon degradation have been found in hydrothermal vent sediments [4]. While archaea have been reported to mediate oxidation of methane and other short-chain alkanes in sediments [5, 26], few have been reported to anaerobically degrade larger hydrocarbons [32]. The finding that Bathyarchaeota and other archaeal phyla are potentially capable of anaerobic degradation of aliphatic or aromatic compounds extends the potential substrate spectrum for

344 archaea. More broadly, building on recent findings [26], this work emphasize that non-methane
345 aliphatic and aromatic compounds could significantly contribute to carbon and energy budgets in
346 these deep-sea settings.

347 Genomic analyses of the 12 MAGs harboring genes for central benzoyl-CoA pathway indicate
348 they have an acetogenic lifestyle. The finding that these organisms use the ATP-consuming class
349 I, not the reversible class II, benzoyl-CoA reductase is surprising. It is generally thought that
350 strict anaerobes must use class II BCRs because the amount of energy available from benzoate
351 oxidation during sulfate reduction or fermentation is not sufficient to support the substantial
352 energetic requirement of the ATP-dependent class I BCR reaction [35]. However, there are
353 reported exceptions to these observations, such as the hyperthermophilic archaeon *Ferroglobus*
354 *placidus* that couples benzoate degradation via the Class I system with iron reduction [35], and
355 fermentative deep-sea Chloroflexi strains DscP3 and Dsc4 that contain genes for class I benzoyl-
356 CoA reductases [37]. Acetogenic oxidation may explain why the Class I reaction is energetically
357 favorable; thermodynamic modelling indicates the free Gibbs energy yield of acetogenic
358 oxidation of benzoate is much higher than its hydrogenogenic or complete oxidation (Table 2).
359 These inferences are in line with mounting evidence that acetogens are important community
360 members in energy-limited seafloor ecosystems [38, 40]. Acetogens may be favored in such
361 ecosystems given their utilization of many organic compounds is thermodynamically favourable,
362 and their relatively high ATP yields [38, 40].

363 Based on the evidence presented here, we propose that acetate and hydrogen are the central
364 intermediates underpinning community interactions and biogeochemical cycling in these deep-
365 sea sediments. Despite the presence of putative acetogens and hydrogenogens, acetate and

366 hydrogen were below the limits of detection in sediment porewater (Supplementary Note 2),
367 indicating both compounds are rapidly turned over by other community members. Consistently,
368 microbial communities encoded the genes for the coupling of acetate consumption to sulfate
369 reduction, organohalide respiration, and acetoclastic methanogenesis, consistent with other
370 studies [49, 53]. Some community members also appear to be capable of H_2 consumption, including
371 through respiratory membrane-bound enzymes and reversible cytosolic enzymes. In turn,
372 hydrogen oxidation can support autotrophic carbon fixation and therefore may provide a
373 feedback loop for regeneration of organic carbon. Moreover, acetate- and hydrogen-oxidizing
374 community members are likely to promote upstream acetogenic and hydrogenogenic degradation
375 of necromass and aliphatic or aromatic compounds. Thermodynamic modelling indicates that
376 maintaining low acetate and hydrogen concentrations in the environment is important for
377 promoting continuous oxidation of organic substrates (Table 2 and Figure 5).

378 **Methods**

379 **Sample selection based on geochemical characterization**

380 The three marine sediment samples used in this study were chosen from among several sites
381 sampled as part of a piston coring seafloor survey in the Eastern Gulf of Mexico, as described
382 previously [20]. Piston cores penetrating 5 to 6 meters below sea floor (mbsf) were sectioned in 20
383 cm intervals on board the research vessel immediately following their retrieval. Three intervals
384 from the bottom half of the core were chosen for geochemical analysis, and were either frozen
385 immediately (for liquid hydrocarbon analyses), or flushed with N_2 and sealed in hydrocarbon-
386 free gas tight metal canisters then frozen until analysis (for gaseous hydrocarbon analysis).
387 Interstitial gas analysis was later performed on the headspace in the canisters using GC with

Flame Ionization Detector (GC-FID). Sediment samples for gas/liquid chromatography and stable isotope analysis were frozen, freeze-dried and homogenized then extracted using accelerated solvent extraction (ACE 200). Extracts were subsequently analyzed using GC/FID, GC/MS, a Perkin-Elmer Model LS 50B fluorometer, and Finnigan MAT 252 isotope mass spectrometry as detailed elsewhere [54]. On the basis of TSF and UCM concentration thresholds described previously [20], core segments from E26 and E29 were qualified and core segments from E44 were disqualified for unambiguous occurrence of thermogenic liquid hydrocarbons. Additionally, interstitial hydrocarbon gases were observed in the core segments of E29. Samples from the surface 0-20 cm interval from these three cores were further analyzed as described below.

Porewater geochemistry

Porewater sulfate and chloride concentrations were measured in a Dionex ICS-5000 reagent-free ion chromatography system (Thermo Scientific, CA, USA) equipped with an anion-exchange column (Dionex IonPac AS22; 4 × 250 mm; Thermo Scientific), an EGC-500 K_2CO_3 eluent generator cartridge and a conductivity detector. Organic acids were analysed in the 0.2 µm filtered sediment porewater using a Thermo RS3000 HPLC fitted with an Ultimate 3000 UV detector. Separation was achieved over an Aminex HPX-87H organic acid column (BioRad, USA) under isocratic conditions (0.05 mM H_2SO_4) at 60°C with a run time of 20 minutes. Organic acids were compared to the retention time of known standards and the limit of detection for acetate was determined to be 2.5 µM.

Metabolomic analysis

For the analysis of metabolites, sediment was centrifuged at 21,100 × g for 10 minutes at room temperature, the supernatant was collected, diluted 1:1 in pure methanol, and filtered through 0.2 µm Teflon syringe filters. Each sediment was subsampled five times to assess technical variability across the sample. Metabolites present in the extracts were separated using ultra high-performance liquid chromatography (UHPLC) performed using a gradient of 20 mM ammonium formate at pH 3.0 in water (solvent A) and 0.1% formic acid (% v/v) in acetonitrile (solvent B) in conjunction with a Syncronis™ HILIC LC column (100mm × 2.1mm x 2.1µm; Thermo Scientific). High-resolution mass spectral data were acquired on a Thermo Scientific Q-Exactive™ HF Hybrid Quadrupole-Orbitrap mass spectrometer coupled to an electrospray ionization source. Data were acquired in negative ion full-scan mode from 50-750 *m/z* at 240,000 resolution with an automatic gain control (AGC) target of 3e6 and a maximum injection time of 200 ms. For MS/MS fragmentation experiments, an isolation window of 1 *m/z* and an AGC target of 1e6 was used with a maximum injection time of 100 ms. Data were analyzed in MAVEN [55]. Metabolites were assigned based on accurate mass and retention times of observed signals relative to standards (where available). Metabolites classified as being involved in the anaerobic degradation of aliphatic and aromatic compound pathways [56], for which metabolites standards are not readily available, were assigned using accurate mass alone. The key benzoate and succinate metabolites were assigning using accurate mass, co-elution and MS/MS fragmentation patterns. To control for variability in total organic content across the sediment samples, metabolite data are presented based on their fractional abundance relative to all observed metabolites (*i.e.* constant sum normalization) and were visualized based on their log fractional abundance [57].

DNA extraction and sequencing

For the three sediment samples, DNA was extracted from 10 g of sediment using the PowerMax Soil DNA Isolation Kit (12988-10, QIAGEN) according to the manufacturer's protocol with minor modifications for the step of homogenization and cell lysis *i.e.*, cells were lysed in PowerMax Bead Solution tubes for 45 s at 5.5 m s^{-1} using a Bead Ruptor 24 (OMNI International). DNA concentrations were assessed using a Qubit 2.0 fluorometer (Thermo Fisher Scientific, Canada). Metagenomic library preparation and DNA sequencing was conducted at the Center for Health Genomics and Informatics in the Cumming School of Medicine, University of Calgary. DNA fragment libraries were prepared by shearing genomic DNA using a Covaris sonicator and the NEBNext Ultra II DNA library preparation kit (New England BioLabs). DNA was sequenced on a ~40 Gb (*i.e.* 130 M reads) mid-output NextSeq 500 System (Illumina Inc.) 300 cycle (2 × 150 bp) sequencing run.

To provide a high-resolution microbial community profile, as well as quantitative insights into microbial community diversity, the three samples were also subjected to 16S rRNA gene amplicon sequencing on a MiSeq benchtop sequencer (Illumina Inc.). DNA was extracted from separate aliquots of the same sediment samples using the DNeasy PowerLyzer PowerSoil kit (MO BIO Laboratories, a Qiagen Company, Carlsbad, CA, USA) and used as the template for different PCR reactions. The v3-4 region of the bacterial 16S rRNA gene and the v4-5 region of the archaeal 16S rRNA gene were amplified using the primer pairs SD-Bact-0341-bS17/SD-Bact-0785-aA21 and SD-Arch-0519-aS15/SD-Arch-0911-aA20, respectively [58] as described previously [20] on a ~15 Gb 600-cycle (2 × 300 bp) sequencing run.

Metagenomic assembly and binning

Raw reads were quality-controlled by (1) clipping off primers and adapters and (2) filtering out artifacts and low-quality reads as described previously [59]. Filtered reads were assembled using metaSPAdes version 3.11.0 [60] and short contigs (<500 bp) were removed. Sequence coverage was determined by mapping filtered reads onto assembled contigs using BBmap version 36 (https://sourceforge.net/projects/bbmap/). Binning of metagenome contigs was performed using MetaBAT version 2.12.1 (--minContig 1500) [61]. Contaminated contigs in the produced bins were further removed based on genomic properties (GC, tetranucleotide signatures, and coverage) and taxonomic assignments using RefineM version 0.0.22 [62]. Resulting bins were further examined for contamination and completeness using CheckM version 1.0.8 with the lineage-specific workflow [24].

Annotation

For MAGs, genes were called by Prodigal (-p meta) [63]. Metabolic pathways were predicted against the KEGG GENES database using the GhostKOALA tool [64] and against the Pfam, TIGRfam and custom HMM databases (https://github.com/banfieldlab/metabolic-hmms) using MetaErg (https://sourceforge.net/projects/metaerg/). The dbCAN web server was used for carbohydrate-active gene identification (cutoffs: coverage fraction: 0.40; e-value: 1e-18) [65]. Genes encoding proteases and peptidases were identified using BLASTp against the MEROPS database release 12.0 (cutoffs: e-value, 1e-20; sequence identity, 30%) [66]. Genes involved in anaerobic hydrocarbon degradation were identified using BLASTp against a custom database (Supplementary Table 8) (cutoffs: e-value, 1e-20; sequence identity, 30%). Hydrogenases were identified and classified using a web-based search using the hydrogenase classifier HydDB [67].

Full-length 16S rRNA genes were reconstructed from metagenomic reads using phyloFlash version 3.1 (https://hrgv.github.io/phyloFlash/) together with the SILVA SSU 132 rRNA database [68]. Diversity calculations were based on separate 16S rRNA gene amplicon library results [20]. Functional and taxonomic McrA gpkgs were used to assess the diversity of methanogens against the metagenomic reads using GraftM with default parameters [69]. Genes encoding the catalytic subunits of hydrogenases, *dsrA*, *acsB*, *assA*, *nmsA* and *bssA* were retrieved from metagenomic reads through diamond BLASTx [70] queries against comprehensive custom databases [39, 67, 71] (cutoffs: e-value, 1e-10; sequence identity, 70%).

Phylogenetic analyses

For taxonomic classification of each MAG, two methods were used to produce genome trees that were then used to validate each other. In the first method the tree was constructed using concatenated proteins of up to 16 syntenic ribosomal protein genes following procedures reported elsewhere [72]; the second tree was constructed using concatenated amino acid sequences of up to 43 conserved single-copy genes following procedures described previously [73]. Both trees were calculated using FastTree version 2.1.9 (-lg -gamma) [74] and resulting phylogenies were congruent. Reference genomes for relatives were accessed from NCBI GenBank, including genomes selected from several recent studies representing the majority of candidate bacterial and archaeal phylogenetic groups [4, 62, 75-78]. The tree in Figure 2 was inferred based on concatenation of 43 conserved single-copy genes (Supplementary Data 1). Specifically, it was built using RAxML version 8 [79] implemented by the CIPRES Science Gateway [80] and it was called as follows: raxmlHPC-HYBRID -f a -n result -s input -c 25 -N 100 -p 12345 -m PROTCATLG -x 12345. The phylogeny resulting from RAxML is consistent with the taxonomic classification of

496 MAGs that resulted from FastTree. Interactive tree of life (iTOL) version 3 [81] was used for tree
497 visualization and modification.

498 For phylogenetic placements of functional genes, sequences were aligned using the ClustalW
499 algorithm included in MEGA7 [82]. All positions with less than 95% site coverage were
500 eliminated. Maximum-likelihood phylogenetic trees were constructed in MEGA7 and
501 evolutionary distances were computed using the Poisson correction method. These trees were
502 bootstrapped with 50 replicates.

503 **Thermodynamic calculations**

504 The values of Gibbs free energy of formation for substances were taken from Madigan et al. [83]
505 and Dolfing et al. [53]. The pH used in all calculations was 8.0 as reported in a previous
506 thermodynamic study of deep buried sediments [40], partial pressure was 300 atm based on water
507 depths at the three sites (http://docs.bluerobotics.com/calc/pressure-depth/), and temperature was
508 set as 4°C to represent deep sea conditions [84]. Calculations and corrections based on actual
509 temperatures, pressure, and concentrations followed accepted protocols for determining reaction
510 kinetics and thermodynamics [85].

511 **Acknowledgements**

512 The work was supported by a Genome Canada Genomics Applications Partnership Program
513 (GAPP) award to C.R.J.H., who is supported by a Campus Alberta Innovates Program Chair.
514 Metabolomics data were acquired by R.A.G. at the Calgary Metabolomics Research Facility
515 (CMRF), which is supported by the International Microbiome Centre and the Canada Foundation
516 for Innovation (CFI-JELF 34986). I.A.L. is supported by an Alberta Innovates Translational

Health Chair. C.G. is supported by an ARC DECRA Fellowship (DE170100310) and an ARC Discovery Project (DP180101762). We thank Xiaoli Dong and Marc Strous for establishing bioinformatics workflows and pipelines, the Centre for Health Genomics and Informatics at University of Calgary for NextSeq sequencing, Alexander Probst for providing the database of 16 syntenic ribosomal proteins, and Nina Dombrowski and Brett Baker for providing a custom blast database for hydrocarbon degradation genes.

Data availability

DNA sequences (amplicon sequences, genomes and raw sequence reads) have been deposited in the NCBI BioProject database with accession number PRJNA415828 and PRJNASUB3936075 (https://www.ncbi.nlm.nih.gov/bioproject/). The authors declare that all other data supporting the findings of this study are available within the article and its supplementary information files, or from the corresponding authors upon request.

Author contributions

X.D. and C.R.J.H. designed the study. X.D. and C.G. processed the data, reconstructed the genomes and performed the genome analyses. X.D., J.D. and D.M. performed thermodynamics analysis. M.C. confirmed phylogenetic analyses of genomes. A.C. and C.L. conducted amplicon sequencing and analyses. J.M.B. and B.B.B. collected samples and performed petroleum geochemistry analyses. J.E.R., R.A.G. and I.A.L. performed metabolomics analyses and data interpretation. X.D., C.G. and C.R.J.H. drafted the manuscript. All authors reviewed the results and participated in the writing of the manuscript.

References

1. Petro, C., Starnawski, P., Schramm, A. & Kjeldsen, K.U. Microbial community assembly in marine sediments. *Aquat Microb Ecol* **79**, 177-195 (2017).
2. Vigneron, A. et al. Comparative metagenomics of hydrocarbon and methane seeps of the Gulf of Mexico. *Sci Rep* **7**, 16015 (2017).
3. Marshall, I.P.G., Karst, S.M., Nielsen, P.H. & Jørgensen, B.B. Metagenomes from deep Baltic Sea sediments reveal how past and present environmental conditions determine microbial community composition. *Mar Genomics* **37**, 58-68 (2018).
4. Dombrowski, N., Seitz, K.W., Teske, A.P. & Baker, B.J. Genomic insights into potential interdependencies in microbial hydrocarbon and nutrient cycling in hydrothermal sediments. *Microbiome* **5**, 106 (2017).
5. Lloyd, K.G. et al. Predominant archaea in marine sediments degrade detrital proteins. *Nature* **496**, 215-218 (2013).
6. Orsi, W.D. Ecology and evolution of seafloor and subseafloor microbial communities. *Nat Rev Microbiol* (2018).
7. Wang, Y. et al. Draft genome of an *Aerophobetes* bacterium reveals a facultative lifestyle in deep-sea anaerobic sediments. *Sci Bull* **61**, 1176-1186 (2016).
8. Orcutt, B.N., Sylvan, J.B., Knab, N.J. & Edwards, K.J. Microbial ecology of the dark ocean above, at, and below the seafloor. *Microbiol Mol Biol Rev* **75**, 361-422 (2011).
9. Inagaki, F. et al. Exploring deep microbial life in coal-bearing sediment down to ~2.5 km below the ocean floor. *Science* **349**, 420-424 (2015).
10. Jørgensen, B.B. & Marshall, I.P. Slow microbial life in the seabed. *Ann Rev Mar Sci* **8**, 311-332 (2016).
11. Jørgensen, B.B. & Boetius, A. Feast and famine--microbial life in the deep-sea bed. *Nat Rev Microbiol* **5**, 770-781 (2007).
12. Arndt, S. et al. Quantifying the degradation of organic matter in marine sediments: A review and synthesis. *Earth-Sci Rev* **123**, 53-86 (2013).
13. Orsi, W.D., Richards, T.A. & Francis, W.R. Predicted microbial secretomes and their target substrates in marine sediment. *Nat Microbiol* **3**, 32-37 (2018).

14. Brooks, J.M. et al. Deep-sea hydrocarbon seep communities: evidence for energy and nutritional carbon sources. *Science* **238**, 1138-1142 (1987).
15. Ijiri, A. et al. Deep-biosphere methane production stimulated by geofluids in the Nankai accretionary complex. *Sci Adv* **4**, eaao4631 (2018).
16. Ruff, S.E. et al. Global dispersion and local diversification of the methane seep microbiome. *Proc Natl Acad Sci U S A* **112**, 4015-4020 (2015).
17. Dong, X. et al. Fermentative Spirochaetes mediate necromass recycling in anoxic hydrocarbon-contaminated habitats. *ISME J* **12**, 2039-2050 (2018).
18. Lin, Y.-S. et al. Towards constraining H_2 concentration in subseafloor sediment: A proposal for combined analysis by two distinct approaches. *Geochim Cosmochim Acta* **77**, 186-201 (2012).
19. Sauvage, J., Flinders, A., Spivack, A. & D'Hondt, S. Global distribution of radiolytic H_2 production in marine sediment and implications for subsurface life. *AGU Fall Meeting Abstracts* (2017).
20. Chakraborty, A. et al. Thermophilic endospores associated with migrated thermogenic hydrocarbons in deep Gulf of Mexico marine sediments. *ISME J* **12**, 1895-1906 (2018).
21. Whiticar, M.J. Carbon and hydrogen isotope systematics of bacterial formation and oxidation of methane. *Chem Geol* **161**, 291-314 (1999).
22. Lapham, L.L., Chanton, J.P., Martens, C.S., Sleeper, K. & Woolsey, J.R. Microbial activity in surficial sediments overlying acoustic wipeout zones at a Gulf of Mexico cold seep. *Geochem Geophy Geosy* **9** (2008).
23. Killops, S.D. & Aljuboori, M.A.H.A. Characterization of the Unresolved Complex Mixture (UCM) in the gas chromatograms of biodegraded petroleums. *Org Geochem* **15**, 147-160 (1990).
24. Parks, D.H., Imelfort, M., Skennerton, C.T., Hugenholtz, P. & Tyson, G.W. CheckM: assessing the quality of microbial genomes recovered from isolates, single cells, and metagenomes. *Genome Res* **25**, 1043-1055 (2015).
25. Boll, M. & Heider, J. in Handbook of Hydrocarbon and Lipid Microbiology. (ed. K.N. Timmis) 1011-1024 (Springer Berlin Heidelberg, Berlin, Heidelberg; 2010).
26. Laso-Perez, R. et al. Thermophilic archaea activate butane via alkyl-coenzyme M formation. *Nature* **539**, 396-401 (2016).

27. Meckenstock, R.U. et al. Anaerobic degradation of benzene and polycyclic aromatic hydrocarbons. *J Mol Microbiol Biotechnol* **26**, 92-118 (2016).
28. Tan, B. et al. Comparative analysis of metagenomes from three methanogenic hydrocarbon-degrading enrichment cultures with 41 environmental samples. *ISME J* **9**, 2028-2045 (2015).
29. Schouw, A. et al. *Abyssivirga alkaniphila* gen. nov., sp. nov., an alkane-degrading, anaerobic bacterium from a deep-sea hydrothermal vent system, and emended descriptions of *Natranaerovirga pectinivora* and *Natranaerovirga hydrolytica*. *Int J Syst Evol Microbiol* **66**, 1724-1734 (2016).
30. Lakhal, R. et al. *Vallitalea guaymasensis* gen. nov., sp. nov., isolated from marine sediment. *Int J Syst Evol Microbiol* **63**, 3019-3023 (2013).
31. Khelifi, N. et al. Anaerobic oxidation of long-chain n-alkanes by the hyperthermophilic sulfate-reducing archaeon, *Archaeoglobus fulgidus*. *ISME J* **8**, 2153-2166 (2014).
32. Rabus, R. et al. Anaerobic Microbial Degradation of Hydrocarbons: From Enzymatic Reactions to the Environment. *J Mol Microbiol Biotechnol* **26**, 5-28 (2016).
33. Porter, A.W. & Young, L.Y. in Advances in Applied Microbiology, Vol. 88. (eds. S. Sariaslani & G.M. Gadd) 167-203 (Academic Press, 2014).
34. Dong, X. et al. Reconstructing metabolic pathways of a member of the genus *Pelotomaculum* suggesting its potential to oxidize benzene to carbon dioxide with direct reduction of sulfate. *FEMS Microbiol Ecol* **93**, fiw254-fiw254 (2017).
35. Holmes, D.E., Risso, C., Smith, J.A. & Lovley, D.R. Genome-scale analysis of anaerobic benzoate and phenol metabolism in the hyperthermophilic archaeon *Ferroglobus placidus*. *ISME J* **6**, 146-157 (2012).
36. Beulig, F., Røy, H., Glombitza, C. & Jørgensen, B.B. Control on rate and pathway of anaerobic organic carbon degradation in the seabed. *Proc Natl Acad Sci U S A* **115**, 367-372 (2018).
37. Sewell, H.L., Kaster, A.K. & Spormann, A.M. Homoacetogenesis in Deep-Sea *Chloroflexi*, as inferred by single-cell genomics, provides a link to reductive dehalogenation in terrestrial *Dehalococcoidetes*. *MBio* **8** (2017).

626 38. He, Y. et al. Genomic and enzymatic evidence for acetogenesis among multiple lineages
627 of the archaeal phylum *Bathyarchaeota* widespread in marine sediments. *Nat Microbiol*
628 **1**, 16035 (2016).
629 39. Adam, P.S., Borrel, G. & Gribaldo, S. Evolutionary history of carbon monoxide
630 dehydrogenase/acetyl-CoA synthase, one of the oldest enzymatic complexes. *Proc Natl*
631 *Acad Sci U S A* **115**, E1166-E1173 (2018).
632 40. Lever, M.A. Acetogenesis in the energy-starved deep biosphere - a paradox? *Front*
633 *Microbiol* **2**, 284 (2011).
634 41. Yu, T. et al. Growth of sedimentary *Bathyarchaeota* on lignin as an energy source. *Proc*
635 *Natl Acad Sci U S A* **115**, 6022-6027 (2018).
636 42. Berney, M., Greening, C., Conrad, R., Jacobs, W.R., Jr. & Cook, G.M. An obligately
637 aerobic soil bacterium activates fermentative hydrogen production to survive reductive
638 stress during hypoxia. *Proc Natl Acad Sci U S A* **111**, 11479-11484 (2014).
639 43. Ma, K., Hao, Z. & Adams, M.W.W. Hydrogen production from pyruvate by enzymes
640 purified from the hyperthermophilic archaeon, *Pyrococcus furiosus*: A key role for
641 NADPH. *FEMS Microbiol Lett* **122**, 245-250 (1994).
642 44. Greening, C. et al. Genomic and metagenomic surveys of hydrogenase distribution
643 indicate H_2 is a widely utilised energy source for microbial growth and survival. *ISME J*
644 **10**, 761 (2015).
645 45. Wagner, T., Koch, J., Ermler, U. & Shima, S. Methanogenic heterodisulfide reductase
646 (HdrABC-MvhAGD) uses two noncubane [4Fe-4S] clusters for reduction. *Science* **357**,
647 699-703 (2017).
648 46. Adhikari, R.R. et al. Hydrogen utilization potential in subsurface sediments. *Front*
649 *Microbiol* **7**, 8 (2016).
650 47. Kawai, M. et al. High frequency of phylogenetically diverse reductive dehalogenase-
651 homologous genes in deep subseafloor sedimentary metagenomes. *Front Microbiol* **5**, 80
652 (2014).
653 48. Carr, S.A. et al. Acetoclastic Methanosaeta are dominant methanogens in organic-rich
654 Antarctic marine sediments. *ISME J* **12**, 330-342 (2018).
655 49. Liu, Y.F. et al. Metabolic capability and in situ activity of microorganisms in an oil
656 reservoir. *Microbiome* **6**, 5 (2018).

50. Dombrowski, N., Teske, A.P. & Baker, B.J. Expansive microbial metabolic versatility and biodiversity in dynamic Guaymas Basin hydrothermal sediments. *Nat Commun* **9**, 4999 (2018).

51. Baker, B.J., Lazar, C.S., Teske, A.P. & Dick, G.J. Genomic resolution of linkages in carbon, nitrogen, and sulfur cycling among widespread estuary sediment bacteria. *Microbiome* **3**, 14 (2015).

52. Hu, P. et al. Genome-resolved metagenomic analysis reveals roles for candidate phyla and other microbial community members in biogeochemical transformations in oil reservoirs. *MBio* **7**, e01669-01615 (2016).

53. Dolfing, J., Larter, S.R. & Head, I.M. Thermodynamic constraints on methanogenic crude oil biodegradation. *ISME J* **2**, 442-452 (2008).

54. Bernard, B.B. et al. Surface geochemical exploration and heat flow surveys in fifteen (15) frontier Indonesian basins. *Thirty-Second Annual Convention & Exhibition May 2008* (2008).

55. Melamud, E., Vastag, L. & Rabinowitz, J.D. Metabolomic Analysis and Visualization Engine for LC−MS Data. *Anal Chem* **82**, 9818-9826 (2010).

56. Gieg, L.M. & Toth, C.R.A. in Anaerobic Utilization of Hydrocarbons, Oils, and Lipids. (ed. M. Boll) 1-30 (Springer International Publishing, Cham; 2017).

57. Durbin, B. & Rocke, D.M. Approximate variance-stabilizing transformations for gene-expression microarray data. *Bioinformatics* **19**, 966-972 (2003).

58. Klindworth, A. et al. Evaluation of general 16S ribosomal RNA gene PCR primers for classical and next-generation sequencing-based diversity studies. *Nucleic Acids Research* **41**, e1-e1 (2013).

59. Kleiner, M. et al. Assessing species biomass contributions in microbial communities via metaproteomics. *Nat Commun* **8**, 1558 (2017).

60. Nurk, S., Meleshko, D., Korobeynikov, A. & Pevzner, P.A. metaSPAdes: a new versatile metagenomic assembler. *Genome Res* **27**, 824-834 (2017).

61. Kang, D.D., Froula, J., Egan, R. & Wang, Z. MetaBAT, an efficient tool for accurately reconstructing single genomes from complex microbial communities. *PeerJ* **3**, e1165 (2015).

687 62. Parks, D.H. et al. Recovery of nearly 8,000 metagenome-assembled genomes
688 substantially expands the tree of life. *Nat Microbiol* **2**, 1533-1542 (2017).
689 63. Hyatt, D. et al. Prodigal: prokaryotic gene recognition and translation initiation site
690 identification. *BMC Bioinformatics* **11**, 119 (2010).
691 64. Lombard, V., Golaconda Ramulu, H., Drula, E., Coutinho, P.M. & Henrissat, B. The
692 carbohydrate-active enzymes database (CAZy) in 2013. *Nucleic Acids Res* **42**, D490-495
693 (2014).
694 65. Yin, Y. et al. dbCAN: a web resource for automated carbohydrate-active enzyme
695 annotation. *Nucleic Acids Res* **40**, W445-451 (2012).
696 66. Rawlings, N.D. et al. The MEROPS database of proteolytic enzymes, their substrates and
697 inhibitors in 2017 and a comparison with peptidases in the PANTHER database. *Nucleic*
698 *Acids Res* **46**, D624-D632 (2018).
699 67. Søndergaard, D., Pedersen, C.N. & Greening, C. HydDB: A web tool for hydrogenase
700 classification and analysis. *Sci Rep* **6**, 34212 (2016).
701 68. Quast, C. et al. The SILVA ribosomal RNA gene database project: improved data
702 processing and web-based tools. *Nucleic Acids Res* **41**, D590-596 (2013).
703 69. Boyd, J.A., Woodcroft, B.J. & Tyson, G.W. GraftM: a tool for scalable, phylogenetically
704 informed classification of genes within metagenomes. *Nucleic Acids Res* **46**, e59 (2018).
705 70. Buchfink, B., Xie, C. & Huson, D.H. Fast and sensitive protein alignment using
706 DIAMOND. *Nat Methods* **12**, 59 (2014).
707 71. Anantharaman, K. et al. Expanded diversity of microbial groups that shape the
708 dissimilatory sulfur cycle. *ISME J* **12**, 1715-1728 (2018).
709 72. Tully, B.J., Sachdeva, R., Graham, E.D. & Heidelberg, J.F. 290 metagenome-assembled
710 genomes from the Mediterranean Sea: a resource for marine microbiology. *PeerJ* **5**,
711 e3558 (2017).
712 73. Kato, S. et al. Genome-enabled metabolic reconstruction of dominant chemosynthetic
713 colonizers in deep-sea massive sulfide deposits. *Environ Microbiol* **20**, 862-877 (2018).
714 74. Price, M.N., Dehal, P.S. & Arkin, A.P. FastTree 2--approximately maximum-likelihood
715 trees for large alignments. *PLoS One* **5**, e9490 (2010).
716 75. Anantharaman, K. et al. Thousands of microbial genomes shed light on interconnected
717 biogeochemical processes in an aquifer system. *Nat Commun* **7**, 13219 (2016).

718 76. Zaremba-Niedzwiedzka, K. et al. Asgard archaea illuminate the origin of eukaryotic
719 cellular complexity. *Nature* **541**, 353-358 (2017).
720 77. Probst, A.J. et al. Differential depth distribution of microbial function and putative
721 symbionts through sediment-hosted aquifers in the deep terrestrial subsurface. *Nat*
722 *Microbiol* **3**, 328-336 (2018).
723 78. Hug, L.A. et al. A new view of the tree of life. *Nat Microbiol* **1**, 16048 (2016).
724 79. Stamatakis, A. RAxML version 8: a tool for phylogenetic analysis and post-analysis of
725 large phylogenies. *Bioinformatics* **30**, 1312-1313 (2014).
726 80. Miller, M.A., Pfeiffer, W. & Schwartz, T. Creating the CIPRES Science Gateway for
727 inference of large phylogenetic trees. *2010 Gateway Computing Environments Workshop*
728 *(GCE)*, 1-8 (2010).
729 81. Letunic, I. & Bork, P. Interactive tree of life (iTOL) v3: an online tool for the display and
730 annotation of phylogenetic and other trees. *Nucleic Acids Res* **44**, W242-245 (2016).
731 82. Kumar, S., Stecher, G. & Tamura, K. MEGA7: Molecular Evolutionary Genetics
732 Analysis Version 7.0 for Bigger Datasets. *Mol Biol Evol* **33**, 1870-1874 (2016).
733 83. Madigan, M.T., Martinko, J.M. & Parker, J. Brock biology of microorganisms, Vol. 13.
734 (Pearson, 2017).
735 84. Xu, W.Y., Lowell, R.P. & Peltzer, E.T. Effect of seafloor temperature and pressure
736 variations on methane flux from a gas hydrate layer: Comparison between current and
737 late Paleocene climate conditions. *J Geophys Res-Sol Ea* **106**, 26413-26423 (2001).
738 85. Dolfing, J. in Hydrocarbon and Lipid Microbiology Protocols. (eds. T.J. McGenity, K.N.
739 Timmis & B. Nogales Fernández) 155-163 (Springer Berlin Heidelberg, Berlin,
740 Heidelberg; 2015).

741 **Tables and Figures**

742 **Table 1 Geochemical description of sediment samples from Sites E26, E29 and E44.** TSF
743 Max: total scanning fluorescence maximum intensity. UCM: unresolved complex mixture. Σn-
744 Alk: sum of C_{15}-C_{34} n-alkanes. ΣAlk Gas: total alkane gases. C_{2+} Alk: sum of alkane gases larger
745 than methane. T/D: thermogenic/diagenetic n-alkane ratio.

746

Core ID	***Site E26***	***Site E29***	***Site E44***
Latitude (N)	26.59	27.43	26.28
Longitude (W)	87.51	86.01	86.81
Water depth (km)	2.8	3.2	3.0
Total Scanning Fluorescence MAX	57326.7	26738.3	13502.3
Unresolved Complex Mixture (μg g^{-1})	32	13	7.3
Σn-Alkanes (ng g^{-1})	2845.3	2527	1045
Thermogenic/Diagenetic Ratio	1.0	2.6	0.8
ΣAlkane Gas (ppm)	9	36012	9.9
C_{2+} Alkanes (ppm)	0.3	17.5	0.5
$C_1/(C_2+C_3)$	NA	3974.2	NA
$\delta^{13}CH_4$ (‰, vs. PDB)*	NA	-85.1	NA

747
748
749
750
751
752

753 * The $\delta^{13}CH_4$ values in Site E26 and E29 could not be determined due to low methane
754 concentration, which can be approximated by subtracting C_{2+} Alkanes from ΣAlkane Gas.

Table 2 Thermodynamic parameters and Gibbs free energies for anaerobic benzoate and hexadecane degradation scenarios in deep-sea sediments.

Substrates	Reaction types	Reactions	ΔG^o (kJ)	ΔH^o (kJ)	$\Delta G^o_{4,300}$ (kJ)*
Hexadecane	1. Hydrogenogenic oxidation	$C_{16}H_{34} + 16H_2O \rightarrow 8CH_3COO^- + 17H_2 + 8H^+$	1089.1	1069.8	753.3
	2. Acetogenic oxidation	$C_{16}H_{34} + 8.5HCO_3^- \rightarrow 12.25CH_3COO^- + 3.75H^+ + H_2O$	176.3	98.4	133.9
	3. Complete oxidation	$C_{16}H_{34} + 12.25SO_4^{2-} \rightarrow 16HCO_3^- + 12.25HS^- + H_2O + 3.75H^+$	-407.3	24.9	-653.3
Benzoate	4. Hydrogenogenic oxidation	$C_7H_5O_2^- + 7H_2O \rightarrow 3CH_3COO^- + HCO_3^- + 3H_2 + 3H^+$	120.9	117.4	12.8
	5. Acetogenic oxidation	$C_7H_5O_2^- + 0.5HCO_3^- \rightarrow 3.75CH_3COO^- + 2.25H^+$	-846.3	-1091.3	-950.3
	6. Complete oxidation	$C_7H_5O_2^- + 3.75SO_4^{2-} + 4H_2O \rightarrow 7HCO_3^- + 3.755HS^- + 2.25H^+$	-76.2	29.4	-230.7

* The Gibbs free energies were calculated for deep-sea conditions of 4 °C, 300 atm, and 2 mM bicarbonate concentrations [40].

Figure 1 Relative frequency of metagenomic sequence reads for different marker genes at Sites E26, E29 and E44. (a) Community composition based on reconstruction of full-length 16S rRNA genes from the metagenomes. Eukaryotes and unassigned reads are not shown. (b) Relative occurrences of hydrogenases with different metal cofactors. (c) Relative abundance of different subtypes of NiFe hydrogenases. (d) Relative abundance of *mcrA* genes indicative of different types of methanogenesis.

Figure 2 Phylogenetic placement of 82 reconstructed metagenome-assembled genomes. A maximum-likelihood phylogenomic tree was built based on concatenated amino acid sequences of 43 conserved single copy genes using RAxML with the PROTGAMMALG model. Sequences of Altiarchaeales ex4484_43 were used as an outgroup. The scale bar represents 1 amino acid substitution per sequence position. Bootstrap values > 70% are indicated. Blue for Site E26 (E26_binX), red for Site E29 (E29_binY), and green for Site E44 (E44_binZ). The genome sequences used for inferring Figure 2 are available in Supplementary Data 1.

Figure 3 Identification of functional genes or pathways present in MAGs. The presence of genes or pathways are indicated by orange shaded boxes. Gene names: Aor, aldehyde:ferredoxin oxidoreductase; Kor, 2-oxoglutarate/2-oxoacid ferredoxin oxidoreductase; Por, pyruvate:ferredoxin oxidoreductase; Ior, indolepyruvate ferredoxin oxidoreductase; GHs, glycoside hydrolases; AssA, catalytic subunit of alkylsuccinate synthase. CmdA, catalytic subunit of p-cymene dehydrogenase; AhyA, catalytic subunit of alkane C2-methylene hydroxylase; H_2ase, hydrogenase; DsrAB, dissimilatory sulfite reductase. Pathways were indicated as being present if at least five genes in the Embden-Meyerhof-Parnas pathway, three genes in the beta-oxidation pathway, four genes in the Wood-Ljungdahl pathway, and six genes

782 in the TCA cycle were detected. Additional details for the central benzoyl-CoA degradation
783 pathway can be found in Supplementary Figure 5. Lactate and ethanol fermentation are indicated
784 if genes encoding respective dehydrogenases were detected. More details about these functional
785 genes and pathways can be found in the text and in Supplementary Table 6.

786 **Figure 4 Heatmap of metabolites identified in sediment pore water at Sites E26, E29 and**
787 **E44 calculated using log fractional abundance.** Metabolite levels were measured by LC-MS
788 and observed intensities are expressed as the log fractional abundance. Technical replicate
789 numbers (n = 5) from each site are given on the bottom axis. Compound names are listed on the
790 right axis and pathway assignments on the left. Compounds denoted with an asterisk can be
791 intermediates in both anaerobic and aerobic metabolic pathways.

792 **Figure 5 Thermodynamic constraints on anaerobic benzoate and hexadecane degradation**
793 **in deep sea sediments.** Three reactions (Reactions 1, 2 and 4) are illustrated as taken from Table
794 2 where $\Delta G^{o}_{4,\,300} > 0$. Thermodynamics for each reaction are indicated by a line in its
795 corresponding color. If $\Delta G^{o} < 0$, the reaction is energetically favorable (indicated by arrow), and
796 if $\Delta G^{o} > 0$ the reaction is assumed not to occur. In the studied environment (outlined in the
797 shaded area), hydrogen concentrations fall below 1 µM while acetate concentrations are below
798 2.5 µM. The graph shows that ΔG^{o} for three reactions are all negative when both actual
799 concentrations of acetate and hydrogen are taken into consideration.

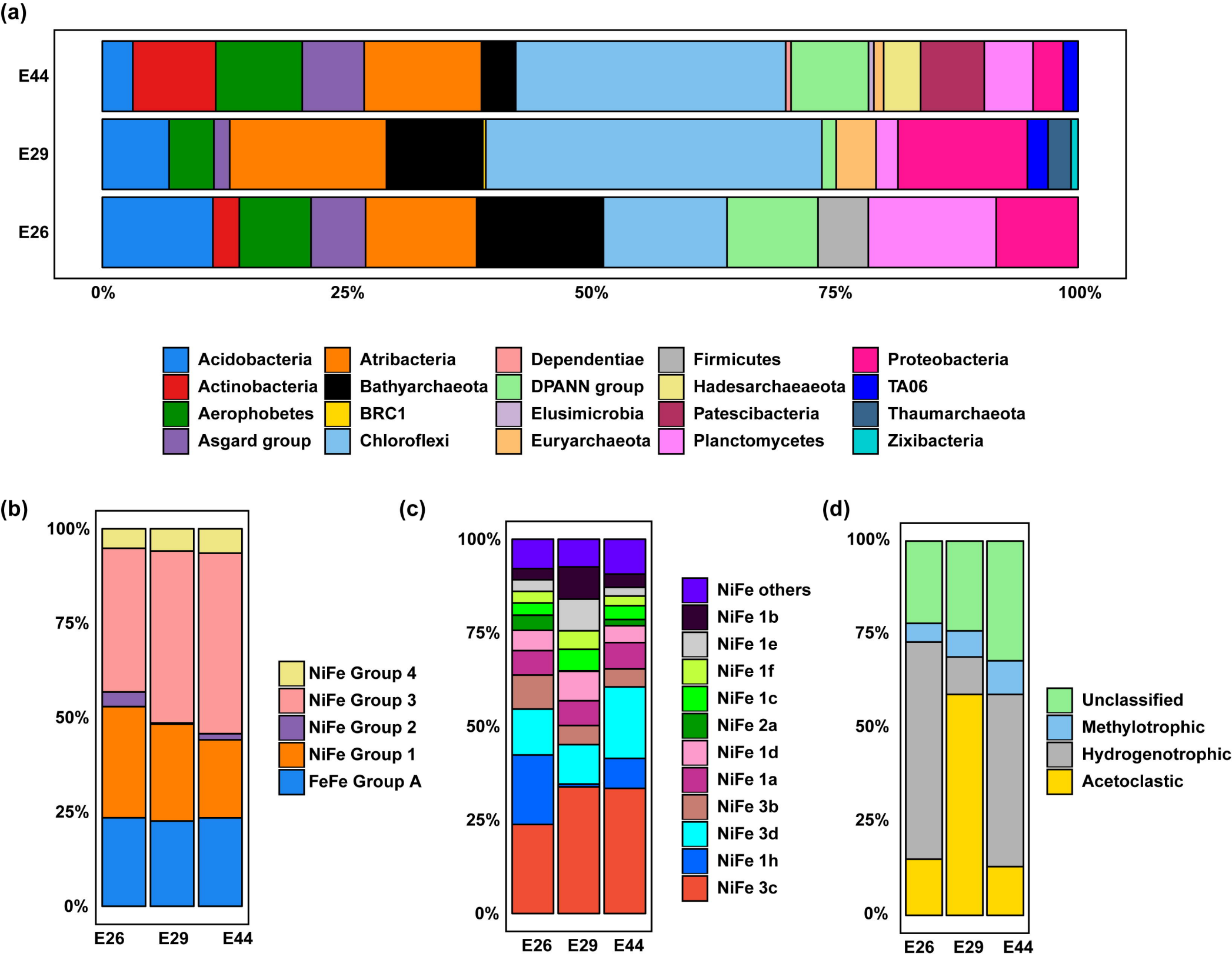
(a)
E44
E29
E26
0%
25%
50%
75%
100%
Acidobacteria
Actinobacteria
Aerophobetes
Asgard group
Atribacteria
Bathyarchaeota
BRC1
Chloroflexi
Dependentiae
DPANN group
Elusimicrobia
Euryarchaeota
Firmicutes
Hadesarchaeaeota
Patescibacteria
Planctomycetes
Proteobacteria
TA06
Thaumarchaeota
Zixibacteria
(b)
100%
75%
50%
25%
0%
E26
E29
E44
NiFe Group 4
NiFe Group 3
NiFe Group 2
NiFe Group 1
FeFe Group A
(c)
100%
75%
50%
25%
0%
E26
E29
E44
NiFe others
NiFe 1b
NiFe 1e
NiFe 1f
NiFe 1c
NiFe 2a
NiFe 1d
NiFe 1a
NiFe 3b
NiFe 3d
NiFe 1h
NiFe 3c
(d)
100%
75%
50%
25%
0%
E26
E29
E44
Unclassified
Methylotrophic
Hydrogenotrophic
Acetoclastic

Asgard
Bathyarchaeota
Euryarchaeota
Dependentiae
Planctomycetes
Aminicenantes
Sulfuricurvum
Gammaproteobacteria
Desulfobacteraceae
Zixibacteria
TA06
Stahlbacteria
Cloacimonas
Elusimicrobia
Aerophobetes
Atribacteria
Actinobacteria
Woesebacteria
Patescibacteria
Anaerolineaceae
Dehalococcoidia
Bathyarchaeota JdFR_09
Bathyarchaeota RBG_16_57_9
Bathyarchaeota NP77
Bathyarchaeota B24_2
Bathyarchaeota BA2
Lokiarchaeota CR_4
Lokiarchaeum sp GC14_75
Thorarchaeota SMTZ1-83
Thorarchaeota MP11T_1
Heimdallarchaeota LC_2
Heimdallarchaeota AB_125
TM6 RIFCSPHIGHO2_12_FULL_32_22
TM6 RIFCSPHIGHO2_12_FULL_38_8
Dependentiae UBA6230
Planctomycetes UBA1135
Planctomycetes UBA1662
Planctomycetes UBA647
Aminicenantes 4484_214
Aminicenantes RBG_13_62_12
Sulfuricurvum GWF2_44_89_gwf2
Sulfurovum UBA5198
Ruthia sp. UBA2013
Gammaproteobacteria RBG_16_57_12
Thiotrichaceae UBA5859
Desulfobacterales CG23
Desulfobacteraceae UBA5616
Desulfobacteraceae 4484_190.2
Desulfobacteraceae 4572_20
Zixibacteria SM23-81
Zixibacteria RBG_16_43_9
Zixibacteria DG_27_17789
TA06 SM1_40
TA06 DG_26_17254
WOR-3 UBA1063
WOR-3 4484_100
WOR-3 SM23_60
WOR-3 UBA3072
Cloacimonas 4484_209
Elusimicrobia UBA6262
Elusimicrobia CG03_land_8_20
Aerophobus_profundus_SCGC_AAA252-L23
Aerophobetes AeroCD12_1
Aerophobetes JGI_0000014_C22
Aerophobetes SCGC_AAA255_F10
Atribacteria UBA6251
Atribacteria UBA3950
Atribacteria 4572_76
Actinobacteria UBA2594
Actinobacteria UBA1414
Actinobacteria RBG_19FT
Actinobacteria CG08
Woesebacteria RIFOXYA1 FULL 40 18
Woesebacteria RBG_16_39_89
Nealsonbacteria CG08_land
Nealsonbacteria CG18_big_fil
Anaerolineales UBA3082
Anaerolineae SM23 84
Anaerolineales UBA5069
Anaerolineales UBA3071
Anaerolineaceae 4572_32.1
Anaerolineae SG8_19
Anaerolineaceae UBA2796
Anaerolineales UBA5838
Anaerolineaceae UBA6092
Anaerolineae SM23_63
Dehalococcoidia UBA2979
Dehalococcoidia UBA826
Dehalococcoidia UBA6926
Dehalococcoidia SM23_28_2
Dehalococcoidia DG_18
Dehalococcoidia UBA5620
Dehalococcoidia UBA6803
Dehalococcoidia UBA2768
Dehalococcoidia SG8-51_3
Dehalococcoidia UBA5760
Dehalococcoidia UBA2145
Hadesarchaea DG-33-1
Hadesarchaea DG-33
Hadesarchaea CG08
Thermoplasmatales ex4484_6
Methanomassiliicoccales UBA149
Altiarchaeales ex4484_43
E29_bin46
E44_bin34
E44_bin77
E44_bin6
E29_bin63
E44_bin85
E44_bin4
E44_bin43
E26 bin22
E29_bin60
E29_bin53
E26_bin4
E29_bin39
E26_bin1
E44_bin54
E44_bin86
E44_bin52
E44_bin17
E44_bin39
E29_bin74
E44_bin49
E29_bin11
E29_bin47
E44_bin83
E26_bin21
E29_bin29
E26_bin20
E44_bin91
E29_bin5
E29_bin65
E29_bin18
E29_bin17
E29_bin49
E29_bin36
E44_bin18
E44_bin36
E29_bin50
E29_bin14
E44_bin50
E29_bin43
E44_bin80
E44_bin20
E44_bin3
E29_bin78
E29_bin52
E29_bin28
E44_bin7
E44_bin65
E26_bin6
E29_bin25
E29_bin7
E29_bin77
E44_bin5
E26_bin3
E44_bin24
E29_bin16
E29_bin31
E44_bin74
E26_bin7
E29_bin35
E29_bin24
E44_bin32
E44_bin81
E29_bin2
E44_bin56
E44_bin26
E29_bin44
E29_bin3
E29_bin15
E44_bin27
E26_bin16
E44_bin10
E29_bin54
E29_bin1
E29_bin75
E44_bin89
E29_bin42
E44_bin88
E44_bin46
E44_bin29
1

Extracellular peptidases
Aminotransferase
Por/Kor/Aor/Ior
Extracellular GHs
Embden−Meyerhof pathway
Beta oxidation pathway
AssA
CmdA/AhyA
Benzoyl−CoA degradation
Wood−Ljungdahl pathway
TCA cycle
Acetate production
Lactate fermentation
Ethanol fermentation
Reductive dehalogenase
FeFe Group A H_2ase
NiFe evolving H_2asee
NiFe uptake H_2ase
NiFe bidirectional H_2ase
Heterodisulfide reductase
DsrAB

Completeness
90
80
70
60

Aerophobetes_E26_bin6
Aminicenantes_E26_bin21
Anaerolineales_E26_bin7
Bathyarchaeota_E26_bin22
Bathyarchaeota_E26_bin4
Dehalococcoidia_E26_bin16
Gammaproteobacteria_E26_bin20
Hadesarchaea_E26_bin1
Woesebacteria_E26_bin3

Anaerolineales_E29_bin16
Anaerolineales_E29_bin24
Anaerolineales_E29_bin35
Bathyarchaeota_E29_bin39
Bathyarchaeota_E29_bin53
Bathyarchaeota_E29_bin60
Dehalococcoidia_E29_bin2
Dehalococcoidia_E29_bin3
Dehalococcoidia_E29_bin42
Dehalococcoidia_E29_bin44
Dehalococcoidia_E29_bin54
Dehalococcoidia_E29_bin73
Dehalococcoidia_E29_bin75
Heimdallarchaeota_E29_bin46
Lokiarchaeota_E29_bin63
Actinobacteria_E29_bin7
Actinobacteria_E29_bin77
Aerophobetes_E29_bin25
Aerophobetes_E29_bin28
Aerophobetes_E29_bin52
Aerophobetes_E29_bin78
Aminicenantes_E29_bin11
Aminicenantes_E29_bin47
Aminicenantes_E29_bin74
Cloacimonetes_E29_bin43
Dehalococcoidia_E29_bin15
Desulfobacteraceae_E29_bin18
Desulfobacteraceae_E29_bin5
Desulfobacteraceae_E29_bin65
Methanomassiliicoccales_E29_bin30
Patescibacteria_E29_bin31
Stahlbacteria_E29_bin14
Stahlbacteria_E29_bin50
Sulfurovum_E29_bin29
TA06_E29_bin36
Zixibacteria_E29_bin17
Zixibacteria_E29_bin49

Anaerolineales_E44_bin24
Anaerolineales_E44_bin32
Anaerolineales_E44_bin81
Bathyarchaeota_E44_bin4
Bathyarchaeota_E44_bin43
Dehalococcoidia_E44_bin10
Dehalococcoidia_E44_bin26
Dehalococcoidia_E44_bin27
Dehalococcoidia_E44_bin29
Dehalococcoidia_E44_bin46
Dehalococcoidia_E44_bin56
Dehalococcoidia_E44_bin88
Dehalococcoidia_E44_bin89
Heimdallarchaeota_E44_bin34
Lokiarchaeota_E44_bin85
Thorarchaeota_E44_bin77
Actinobacteria_E44_bin5
Aerophobetes_E44_bin3
Aerophobetes_E44_bin7
Aerophobetes_E44_bin92
Aminicenantes_E44_bin49
Aminicenantes_E44_bin83
Atribacteria_E44_bin65
Cloacimonetes_E44_bin50
Cloacimonetes_E44_bin80
Dependentiae_E44_bin17
Dependentiae_E44_bin52
Desulfobacteraceae_E44_bin91
Elusimicrobia_E44_bin20
Hadesarchaea_E44_bin54
Hadesarchaea_E44_bin86
Patescibacteria_E44_bin74
Planctomycetes_E44_bin39
Stahlbacteria_E44_bin36
TA06_E44_bin18
Thorarchaeota_E44_bin6

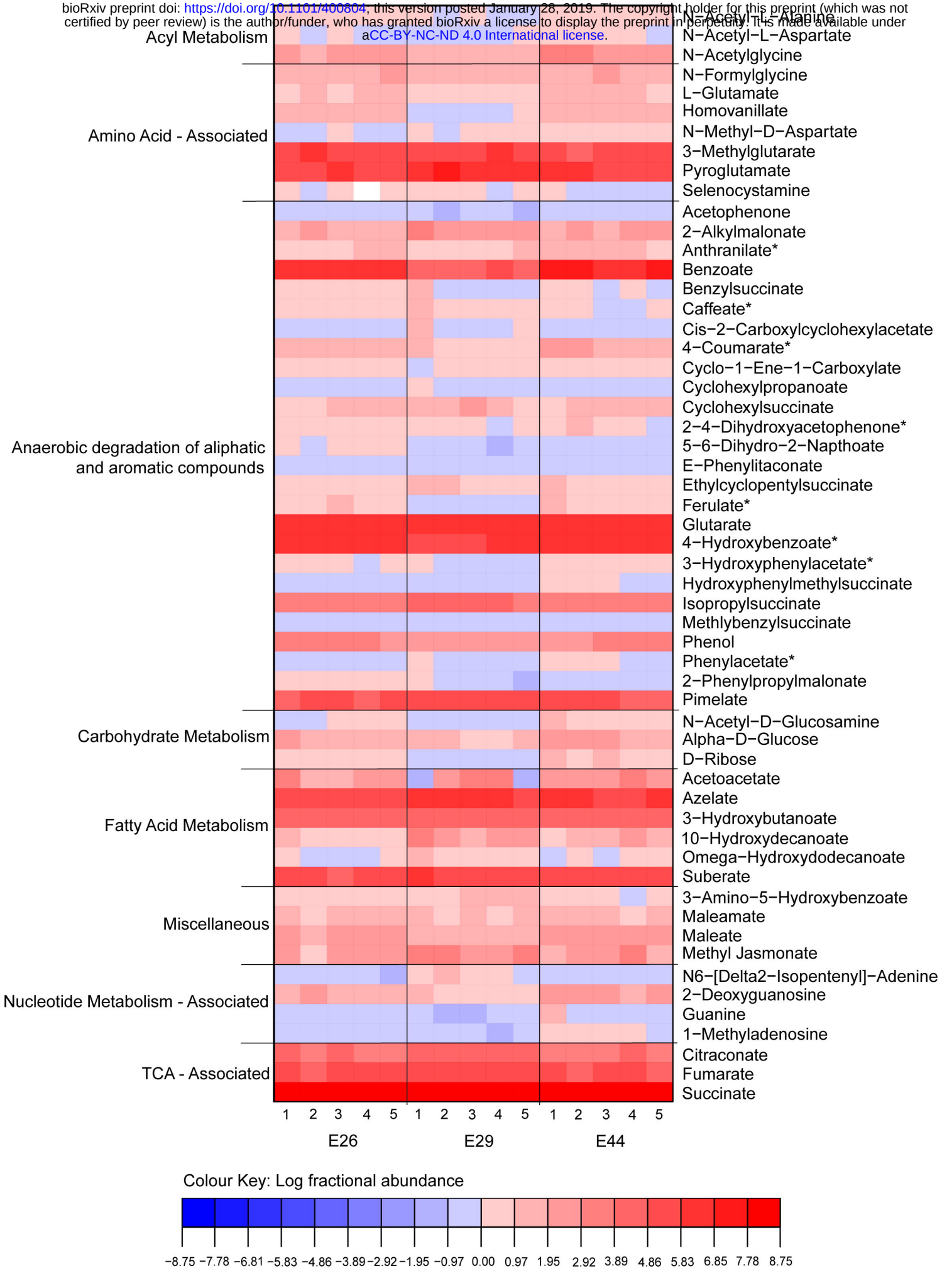

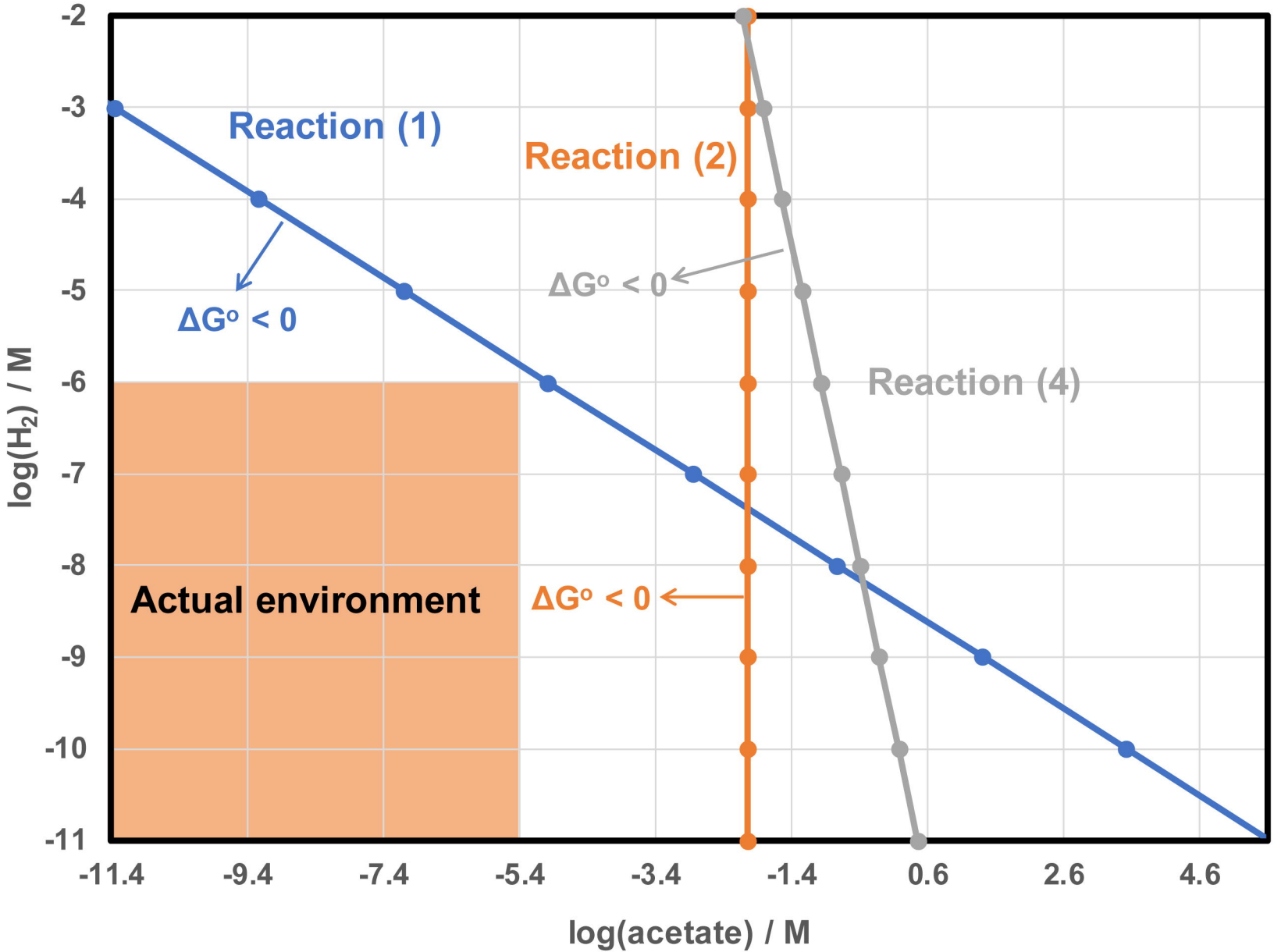
Reaction (1)
Reaction (2)
Reaction (4)
ΔG° < 0
ΔG° < 0
ΔG° < 0
Actual environment
-2
-3
-4
-5
-6
-7
-8
-9
-10
-11
log(H2) / M
-11.4
-9.4
-7.4
-5.4
-3.4
-1.4
0.6
2.6
4.6
log(acetate) / M